Fine-Scale Evaluation of Rainfall from TV-Sats: A New Method for Water Monitoring and Flash Flood Prevention

François Mercier[1,2], Nawal Akrour[1], Laurent Barthès[1], Cécile Mallet[1], and Ruben Hallali[1,3]

[1]Laboratoire Atmosphères, Milieux, Observations Spatiales

[2]Now: Centre National de Recherches Météorologiques, France

[3]Now: Direction des Systèmes d'Observation, Météo France, France
E-mail: francois.mercier@meteo.fr, nawal.akrour@latmos.ipsl.fr
laurent.barthes@latmos.ipsl.fr cecile.mallet@latmos.ipsl.fr
ruben.hallali@meteo.fr

Abstract

In this paper we present a method for rebuilding rainfall maps at high resolution (500 m × 500 m, 1 min). This method is based on the assimilation of opportunistic measurements of the attenuation that affects the signals coming from TV satellites in a model of spatiotemporal advection of rainfall fields. At the frequencies used (Ku band), the attenuation affecting the signals in the atmosphere is mainly due to rain. We set a sensor (field analyzer) on the ground, and then measured the mean rainfall over the link. This method was applied to a simulated network of sensors. These simulated sensors were realistically set over the Paris area, on a zone assumed to be typical of an area with high socio-economic issues (flood prevention, water resources management). We compared the simulated rainfall maps with the maps rebuilt by our algorithm. We then showed the feasibility of our approach for measuring the rainfall in urban areas with high resolution.

1. Introduction

This paper presents a new method for retrieving rain maps (namely, two-dimensional fields of rainfall rates on the ground, in mm/h, at successive time steps) at fine spatiotemporal resolution (typically 500 m × 500 m and 1 min). This method uses the measurement of the attenuation due to rain affecting electromagnetic waves emitted in the Ku band by geosynchronous TV satellites.

Traditionally, these rain maps are produced from rain-gauge records or weather-radar data, or from a combination of both types of measurements. However, both of these instruments have weaknesses. Rain gauges only provide point measurements. The very high spatiotemporal variability of rain implies having a very dense rain-gauge network to correctly estimate fine-scale rain maps (as well as the total amount of rain over an area, for instance, for hydrological purposes). The deployment of such a dense network implies significant maintenance costs, so that there are now fewer and fewer rain gauges available [1]. Furthermore, radars are blocked by mountains (inter alia), and are very expensive to buy, to sustain, and to use. Mountainous areas as well as developing countries are consequently generally not covered by operational networks. The use of radars in hydrology also raises questions [2].

The use of the attenuation affecting microwave electromagnetic signals as a new way for measuring rain has received increasing attention in the scientific community for about 20 years. Most of the studies on this topic focused on the attenuation of telecommunications microwave signals [1, 3-6]. However, some of them already measured the attenuation of waves coming from geosynchronous TV satellites on the ground [7, 8]. By nature, all these measurements provide information about rainfall that is indirect and integrated in space. Firstly, it is indirect because we measure attenuations, and so we need a way (actually, a power law, see [7] and Section 2 of this paper) to convert these attenuations into rain rates. Secondly, they are integrated because we measure the mean attenuation over an emitter/receiver pathway. These pathways are typically a few kilometers long, whether this is for the telecommunication links or the satellite/Earth links (the attenuation only occurs in rain, so the pathway is restricted to the segment from the base of the clouds or from the freezing level to the ground; see Section 2). Consequently, for retrieving rain maps at fine spatiotemporal resolution (around 1 km or below), we need to couple the raw measurements with a retrieval algorithm.

The first studies on this topic generally restricted the links to their center points, and have used kriging or tomography algorithms to retrieve rain maps [9]. In these algorithms, the measurements at successive time steps are regarded as independent (they do not use a propagation model to explicitly link the successive data). Several studies using very dense measuring networks (and/or data at low time sampling) also proceeded in this way (for instance, [1] produced rainfall maps over the entire Netherlands using telecommunications data and a kriging algorithm).

Reference [5] first used the mathematical framework of data assimilation to post-process telecommunications measurements. Data assimilation roughly consists in using a propagation model (typically, a model that moves the rain fields according to the wind) to link the measurements recorded at successive time steps. The unknown of such a model is the rain map at a given initial time, t_0. We then look for the rain map at t_0 that once propagated by the model best explains the measurements (the attenuations) recorded over a time period. This approach allows working with less-dense networks. The good temporal sampling of the data is used (via the model) to increase the spatial resolution.

The study presented in this paper used attenuations measured from TV satellites emitting in the Ku band (around 12 GHz). It combined these data together with a four-dimensional-variational assimilation algorithm. This approach was applied to real rain case studies recorded in the department of Ardèche, in the southeast of France, during the HyMeX campaign (Hydrological Cycle in the Mediterranean Experiment, [10]). These results were published [11]. We then extended the approach – for now, only on simulated data – to a more-dense and realistic network of attenuation sensors simulating an urban area.

Section 2 of this paper gives more information about the measuring system and the retrieval algorithm. In Section 3 we then present the results obtained with this simulated network.

2. Methodology

2.1 Measuring Device

The Ku frequency band (around 12 GHz) is mainly attenuated in the atmosphere by liquid raindrops [7]. This attenuation consequently mainly occurs in rain (under the clouds or under the freezing level).

The idea is to set sensors on the ground in order to measure the attenuation of microwave signals coming from geosynchronous TV satellites. Figure 1 schematically represents this situation for one sensor. We can see that the recorded attenuation is integrated over Earth/satellite segments a few kilometers long. A precise description of the sensor and of the first post-processing treatment applied to the very raw data (temporal averaging to get a 10 s sampling, with the algorithm able to distinguish the part of the attenuation due to rain from the (small) part due to clouds and other effects) was provided in [7]. We can just notice that these sensors can theoretically be connected to dedicated antennas or to personal antennas, already installed. We then consider in this study that our "raw" data are the attenuations (in decibels, dB) along these Earth/satellite links with a 10 s sampling.

These attenuations are linked to the mean rainfall rate over the link (R, in mm/h) by the power law [7]

$$K = aR^b,$$

with a and b being two coefficients that notably depend on frequency, polarization, and on the drop-size distribution (typically, at 12 GHz, a is around 0.024 and b around 1.1 to 1.2).

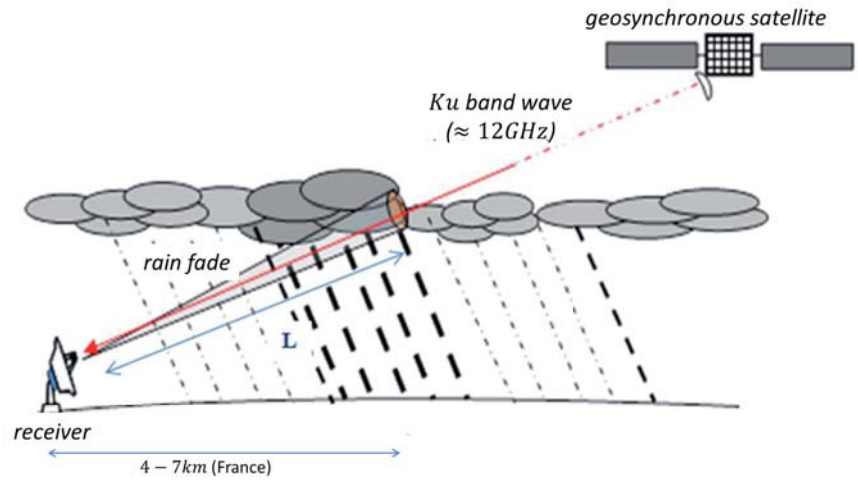

Figure 1. A description of the system that allows measuring the attenuation of satellite signals and that was used in this study ("Ku link").

The purpose of this study was to retrieve rainfall maps by combining such measurements (recorded at successive time steps by several sensors) with a model able to simulate the propagation of the rain fields. Because we wanted to avoid the use of the power law during the execution of the data-assimilation algorithm, we worked with linear attenuations (in dB/km) during the entire process, and converted these linear attenuations into rain rates offline, at the very end of the algorithm. We will nevertheless generally present visual results in terms of rainfall rates.

2.2 Retrieval Algorithm

The 4D-VAR data-assimilation algorithm (see, for instance, [12]) consists in coupling time-distributed observations with a numerical model able to propagate information through time, in order to retrieve values compatible both with the observations (then allowing to fuse them) and with the dynamics included in the model. Consequently, we first have to define a model (typically, the discretization of partial differential equations, PDEs) able to simulate the dynamics of the rainfall fields (or, similarly, of the attenuation fields).

2.2.1 Propagation Model

In this study, we used a simple advection model at constant speed. Let $K(t,x,y)$ be an attenuation field at any time t and any point (x,y) on a plane (we restrict the problem to a plane by assuming that the rain is homogeneous on the vertical columns). Let u and v be the advection speeds to the north and to the east. The partial differential equation driving the propagation of the of the attenuation field is then

$$\frac{\partial K}{\partial t} = u\frac{\partial K}{\partial x} + v\frac{\partial K}{\partial y}.$$

We can note that the assumptions made here are the same as in [11]. We also note that this model, which assumes that rain fields move without any distortion and assumes homogeneous and constant winds, will only be workable, for the spatial resolution considered here, over short time periods (typically, 30 min to 1 h, depending on the topography of the area studied). It could be possible to use a more-complex model (for instance, with non-constant winds), but we would need a dense network of attenuation sensors to estimate its parameters. Such a network was not available in our first study [11], but could be considered for future developments. About the wind parameters (u and v), we showed in [11] that if two sensors are available and wisely set up, the wind parameters can be directly estimated from the time series of attenuations (using a cross-correlation technique). We then assume that these parameters are fully known.

The partial-differential-equation problem is well-posed only if we also define boundary and initial conditions. About the boundary conditions, we assume that no rain enters the considered area during the time period (the inflow is zero). If we retrieve the initial condition $K(0,x,y)$, we would thus be able to estimate the attenuation field at any time and location. This is the goal of the 4D-VAR data-assimilation algorithm.

We finally note that we also have to discretize the partial differential equation for running it. To do so, we use an anti-diffusive scheme proposed by [13]. The discretization steps are 500 m and 1 s.

2.2.2 Data-Assimilation Algorithm

We have defined the dynamics governing the evolution of the attenuation fields, so we can now introduce the 4D-VAR data-assimilation algorithm used to retrieve the initial attenuation field, $K(0,x,y)$, which is the only unknown of the problem. An introduction to data assimilation was provided, for instance, in [12]. This algorithm roughly consists in minimizing a cost function, J, which sums two parts which estimate:

> The gap between the observations available and the initial (unknown) field propagated through the model until the time steps corresponding to the observation records.

There are possibly other terms bringing information about a priori knowledge of the unknown field (the gap between the unknown field and a predefined field, or more general information, for instance, regularization terms).

In this study, we used the following cost function:

$$\mathbf{J}\left(\mathbf{K}^0\right) = \alpha\left\|\mathbf{K}^0 - \mathbf{m}\left(\mathbf{K}^0\right)\right\|^2 + \sum_n \left\|\mathbf{y}^n - \mathbf{H}^n\mathbf{K}^n\right\|^2$$

$\mathbf{K}^0$ is the two-dimensional attenuation field at $t=0$ rewritten under a vector form. $\mathbf{K}^n$ is the attenuation field at time t_n (also under a vector form). $\mathbf{K}^n$ is just the propagation of $\mathbf{K}^0$ until t_n using the discretization of the advection model, called $\mathbf{M}^n$. $\mathbf{H}^n$ is the operator of observations that allows converting the linear attenuations at every grid point into attenuations integrated over the Ku Earth/satellite pathways. For a given Ku link, this operator is a linear combination of the linear attenuations in the grid points "crossed" by the link. The $\mathbf{y}^n$ are the observations at time t_n (the attenuations). $\mathbf{m}\left(\mathbf{K}^0\right)$ is the local average of $\mathbf{K}^0$ (calculated over the nine grid points directly connected to the considered point). Finally, the first part of $\mathbf{J}\left(\mathbf{K}^0\right)$ is a regularization term, while the second one is a term estimating the gap to the observations. For a more detailed

description of this cost function, we can refer to [11]. For minimizing this cost function and so estimating $\mathbf{K}^0$, we have to calculate its gradient. This calculation is made using the adjoint operators (transpose of the linear tangent) of the operator of observations, $\mathbf{H}^n$, and of the model, $\mathbf{M}^n$.

In order to facilitate all these developments, we used the YAO tool, developed at the LOCEAN laboratory (Laboratoire d'Océanographie et du Climat), and described, for instance, in [14]. This tool, written in *C++*, eases the development of 4D-VAR algorithms by writing their components (operator of observations, nonlinear model, etc.) under the form of basic components (analytic operations performed at every grid point and time step). These basic components are linked by a graph describing their connections (for the concept of a modular graph, see [14]). The minimization part of this process is done with the quasi-Newton m1qn3 algorithm developed in [15].

We now have defined the 4D-VAR algorithm that retrieves the attenuation map at the initial time, $\mathbf{K}^0$. Using the model $\mathbf{M}^n$, we can deduce $\mathbf{K}^n$, the attenuation maps at every time. Using the power law linking rain rate and attenuation, we can estimate the rain maps at every time.

3. Results from Simulated Data for an Urban Area

This retrieval algorithm was successfully tested on real but sparse data (one ground receiver measuring the attenuation of the waves coming from four different satellites). The goal of this paper is to evaluate the retrieval algorithm for a denser network of sensors, corresponding to a realistic urban-area situation. Because we did not have experimental data for such an area (it would imply the use of many sensors), we worked with simulated sensors and simulated rain maps. In this section, we first introduce the method employed to simulate all the data needed, and we then present our results.

3.1 Method Employed to Generate the Simulated Data

To run a data-assimilation experiment on simulated data, we successively have to:

1. Choose an area of interest.
2. Define locations for the Ku sensors, in a realistic way.
3. Simulate "true" rain maps, which are the maps we will then try to retrieve with our assimilation algorithm.
4. Simulate a wind (advection speed determined by parameters u and v) to run the advection model.
5. Simulate observations. To do so, from the "true" rain maps, we will use the advection model and the operator of observations. These observations are the attenuations along the links defined at point 2, plus possible instrumental noise.

These five steps allowed simulating what could be measured by a real system for maps of different sizes and

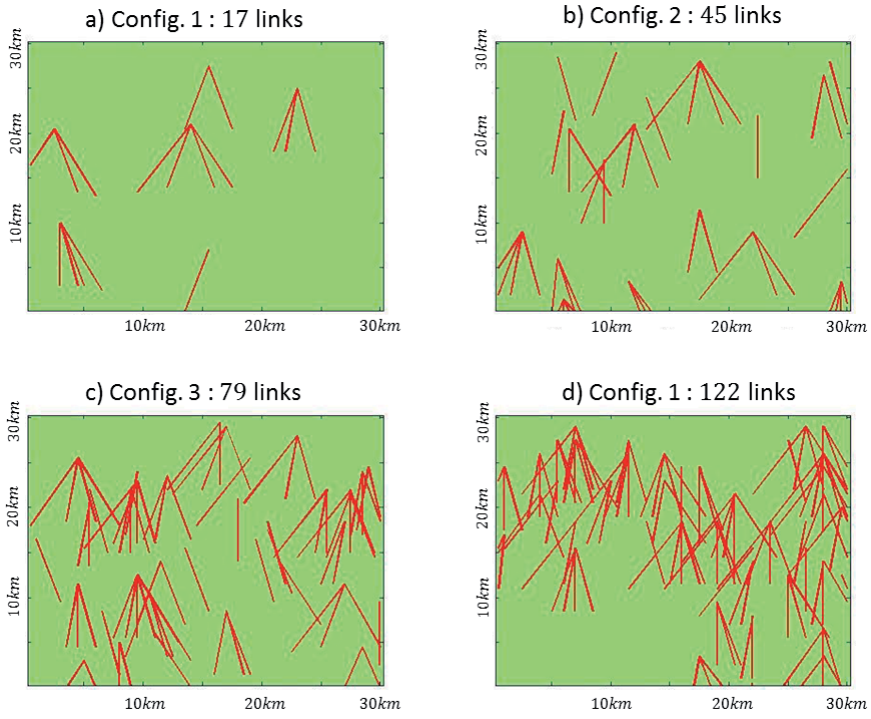

Figure 2. The Ku links used for configurations 1 to 4 in the area of interest.

for different network configurations. We then applied our retrieval algorithm to the simulated observations (created at point 4), and studied the ability of the algorithm to retrieve the rain maps (created at point 3) from these observations. Just before going through the results, we will give some details about these five points.

1. The area studied was located in the Paris area, France. More specifically, it covered a part of the French department of Yvelines, on an area of approximately 30 km × 30 km, centered over the city of Trappes (48.78N, 1.98E). This area is a densely populated area, but the spread of the population is not really homogeneous, with both urban communities and agricultural areas. We could therefore expect areas with dense Ku-sensor networks, and others with almost no sensors available. Moreover, there are different socio-economic impacts of rain in this area. First, the urban areas can be affected by floods caused by the river Seine. Second, water-resource management is important, for both the inhabitants' needs and for agriculture.

2. We then had to define locations for the Ku sensors. Figure 2 shows four configurations tested in this study. In any case, the Ku sensors were set up according to the population density on the considered grid point. All the links were also directed to real satellites available around Paris ([11] listed some of these satellites). We can also note that all the links pointed mainly to the south, because the satellites are geosynchronous, and so located above the equator. From one configuration to another one, we changed the number of available sensors (17, 45, 79, and 122 for configurations 1 to 4). These configurations were thus realistic configurations, depending on the investments made in terms of number of installed sensors.

3. For the rainfall maps, we simulated the map at the initial time, t_0, and we then used the advection model to generate the other maps. To create this individual first map, we used a method developed by [16] that allows simulating realistic two-dimensional rainfall maps. In this study, we worked with the map that is shown in Figure 3. On this map, it was raining over 37% of the grid points, with an average rain rate of 1.1 mm/h and a maximum of 38 mm/h.

4. Concerning the advection parameters, we supposed that the rain cells moved eastward at a speed of 10 m/s, realistic for the Paris area. We therefore had $u = 0$ and $v = 10$ m/s.

5. All the needed parameters of the problem were now defined. We used the wind defined at point 4 in the advection model to move the rain rate of Figure 3 and to get the rain maps at any time. We then transformed these rain maps into linear attenuation maps (power law), and we used the operator of observations to simulate the attenuations along the different links defined in Figure 2. We then possibly added instrumental noise to these data. We thus had observations ready to be used as input to the assimilation algorithm.

We can nevertheless note that in this procedure, we assumed that the numerical model of advection was perfect. We used the same advection model with the same parameters ($u = 0$, $v = 10$ m/s) for both simulating the observations and for running the assimilation model from these observations. The results that follow therefore were representative of cases for which the model was "sufficiently" realistic. This question (what does "sufficiently" mean?) was already asked in our first study on real data [11]. We then showed that we were able to treat four rain events over eight. This value nevertheless depends on the topography, meteorological conditions, and sensor network design, and needs to be carefully studied in any future real data study. An improvement of the model's performance (by using non-constant winds) can also be considered.

We were now ready to run the assimilation model and to compare its output (the rain map at t_0) with the true map of Figure 3.

3.2 Results

3.2.1 Non-Noisy Data: Results According to the Density of Sensors

First, we chose to not add instrumental noise to the simulated data. We also assumed that our observations were

Table 1. The statistical errors produced by the assimilation algorithm compared to the true initial rain map for the experiments shown in Figure 4.

	Entire Map		Rainy Areas		Dry Areas	
	RMSE (mm/h)	Bias (mm/h $\frac{mm}{h}$)	RMSE (mm/h)	Bias (mm/h)	RMSE ($\frac{mm}{h}$ mm/h)	Bias (mm/h)
Config. 1	0.88	–0.09	1.95	–0.75	0.16	+1.16
Config. 2	0.82	–0.10	1.71	–0.24	0.18	+0.18
Config. 3	0.40	+0.01	0.99	–0.98	0.07	+0.07
Config. 4	0.37	–0.01	0.93	–0.11	0.10	+0.10

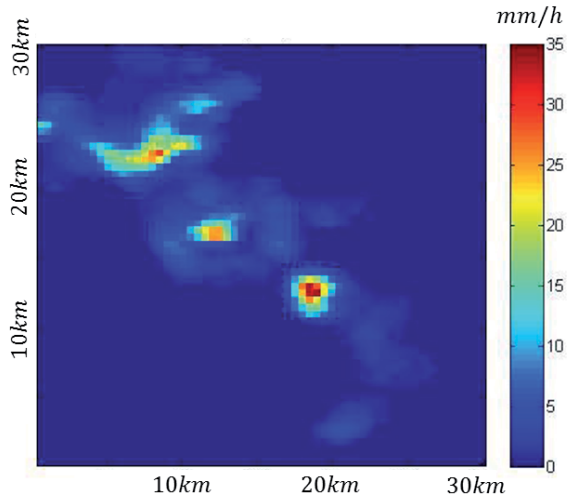

Figure 3. The simulated rain map considered as the true rain map in this study.

sampled at 10 s (as were the real data in [11]). We then tested our algorithm's performance on the four configurations shown in Figure 2, from the sparsest (configuration 1, Figure 2a) to the densest (configuration 4, Figure 2d).

Figure 4 shows the initial true rain map (a) and the four maps retrieved by our algorithm (b to e) for each of these configurations. Table 1 gives several statistical results concerning the errors that our algorithm implied in terms of bias and RMSE (root mean square error) compared to the true map. In Table 1, we also distinguished the areas of the true rain map that were dry from the rainy areas.

Several results could be deduced from these visual and numerical results:

- We noted that only configurations 3 and 4 were able to correctly retrieve the three main rain cells that appeared on the true map (Figure 4). Both configurations 1 and 2 missed the southern rain cell. This was not an unexpected result, because during its eastward advection, this cell only crossed areas with a very low density of population. These areas were consequently not covered (or very sparsely covered) by Ku sensors (Figure 2).

- In any case, the total amount of water that fell over the area was very well retrieved (biases in the third column of Table 1). This was especially true for configurations 3 and 4, when the sensors gave a very good coverage of the entire area. Again, we noted that the bias was slightly negative for configurations 1 and 2 because a part of the rain could not be seen by any sensor.

- The root mean square error decreased when we added links (from configuration 1 to configuration 4). Nevertheless, it remained quite strong from 0.4 mm/h up to 0.8 mm/h for an average rain rate of 1.1 mm/h. However, this could be produced by noise (oscillations) on the initial map as a result of the assimilation algorithm. These oscillations would then be quickly smoothed during the advection (numerical diffusion phenomenon), and so they would not add an important cost in the assimilation cost function. We could again calculate these root mean square errors using the rain maps at any time, instead of only for the initial case. However, the regularization term of the cost function was specifically added in order to limit this effect, so we kept the values calculated from the initial rain maps as an indicator.

- We can note overall (and especially for configurations 3 and 4) that the features (intensity, size, and location) of the true rain maps were very well reproduced by the assimilation-retrieval algorithm.

- Finally, we noted (Table 1) that this algorithm tended to underestimate the rain in rainy areas, and to slightly overestimate the rain in dry areas (we retrieved rain in areas where it did not rain). This is due to the fact that our retrieved maps were smoother than the true map.

In summary, the assimilation algorithm was able to retrieve the true map's features only if there were enough sensors to cover the entire area considered (we retrieved only what was seen). We could nevertheless note that the areas in which the rain rates were poorly retrieved in this study corresponded to sparsely populated areas.

3.2.2 Results on Noisy Observations and Impact of the Time Sampling of Observations

We then studied two phenomena that could decrease the performance of the retrieval algorithm. The first was instrumental noise. The second was the time sampling of the observations. To this end, we added to our simulated observations noise of 0.5 dB, which corresponded to the typical noise affecting the sensor used in [7, 11]. We then performed assimilation experiments with successive time samplings of 10 s (the same as in the previous paragraph), 1 min, and 5 min. In all these tests, we used configuration 3 for the sensor network. This configuration allowed covering all the area studied with as few sensors as possible.

For these experiments, Figure 5 and Table 2 show the same results as the previous Figure 4 and Table 1 (rain maps, biases, root mean square error).

We noted (Figure 5b compared to Figure 4d and Table 2) that if we added noise to the observations, it also added noise to the assimilation outputs. This nevertheless did not affect the good overall retrieval of the features of the true map (for instance, we still retrieved the main rain-cell locations very well). This did not affect the overall bias (+0.05 mm/h with noise, +0.01 mm/h without noise). However, when we added noise, this tended to produce very localized and strong fake rain areas, possibly far from the real rain cells. During the assimilation process, the initial

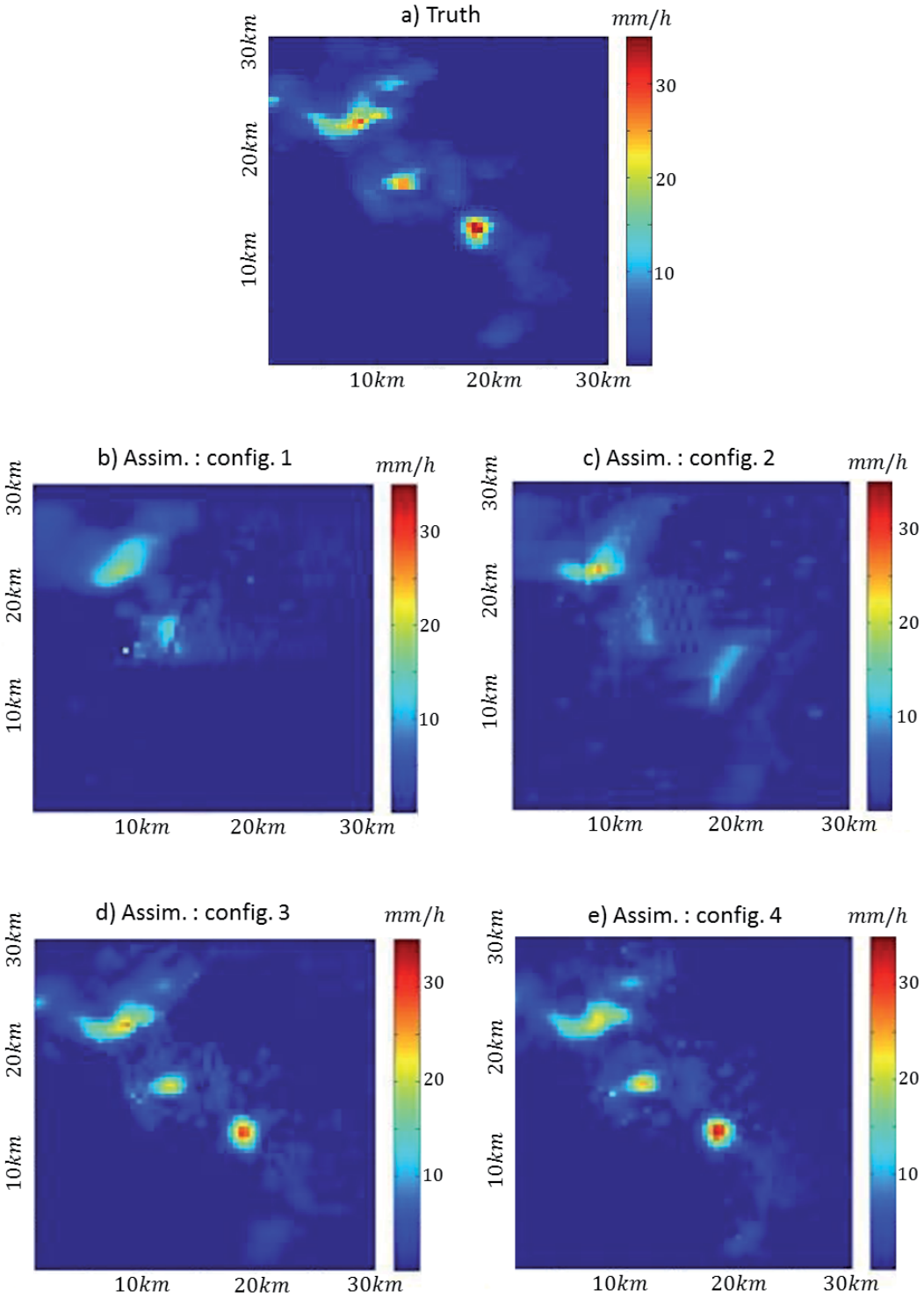

Figure 4. (a) The initial true rain map. (b)-(e) The initial rain maps produced by the assimilation algorithm, for observations with a sampling of 10 s and the four configurations shown in Figure 2.

rain map is advected by the numerical model before being compared to the observations in the cost function. The numerical model immediately (meaning, in a few time steps) smoothes the strong rain gradients appearing on the initial map. Finally, these localized strong gradients will be almost transparent, both in the cost function and in the bias statements.

Now, when we decreased the time sampling (Figures 5c, 5d, and the two last lines of Table 2), we could see that the performance of the algorithm significantly decreased. For instance, the root mean square errors were quite strong (1.52 mm/h for a 5 min time sampling). We also remark that several fake strong rain retrievals (Figure 5d) occurred.

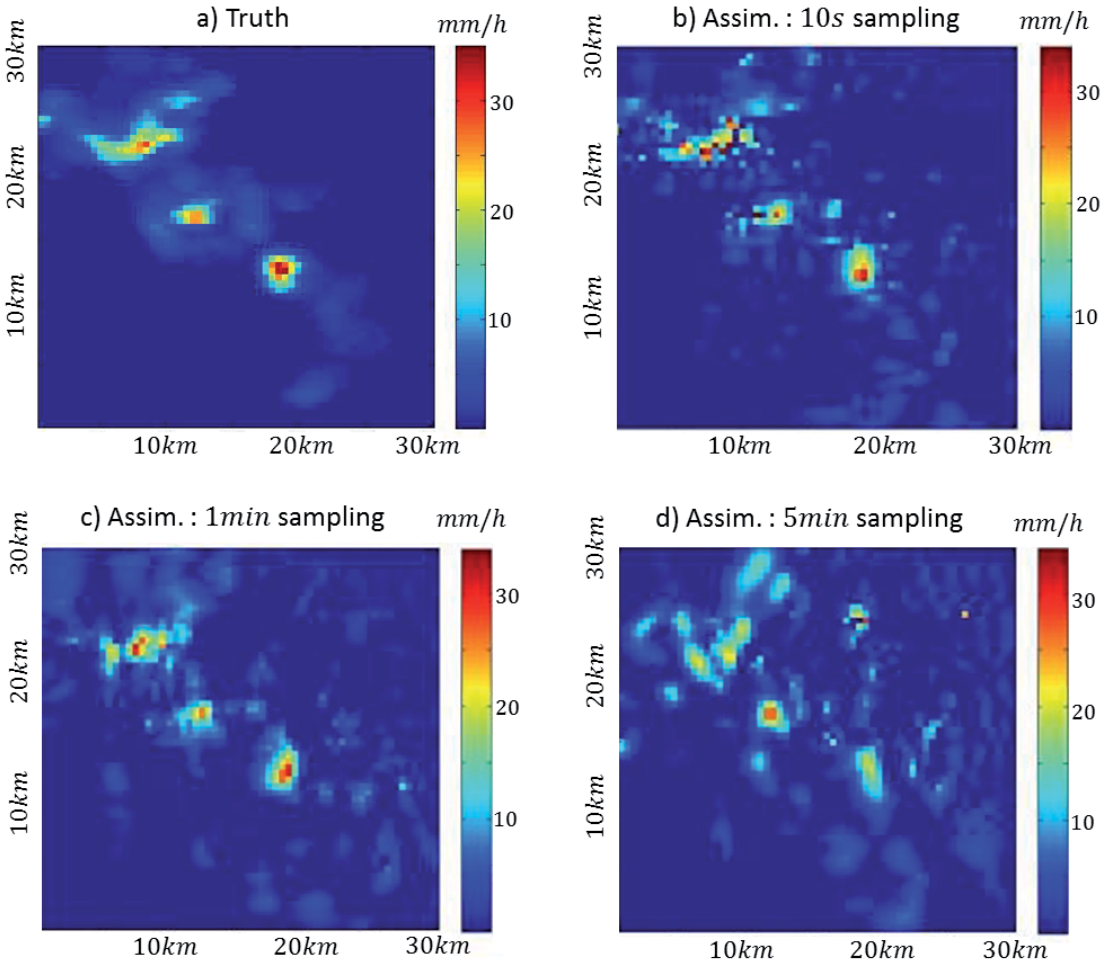

Figure 5. (a) The true initial rain map. (b)-(d) The initial rain maps produced by the assimilation for noisy observations for configuration 3 of Figure 2, with time samplings from 10 s to 5 min for the observations.

To conclude, we noted that 0.5 dB noise in the observations was not troublesome for the algorithm retrievals. The statistical results were almost the same (for instance, we still got low biases). The initial retrieved rain map was noisier, but this noise was very quickly smoothed during the advection process by the model (numerical diffusion). We rather noted that we needed a time sampling better than 1 min (ideally, 10 s if it is possible). If it was 1 min or worse, the quality of the retrievals largely decreased. This was not an unexpected result: one of the main principles of this technique is to use the good time sampling of the measurements to produce (via the model) maps with high spatial resolution. If we do not have this good time sampling, the algorithm fails. These simulations have shown the ability of the method to produce rain maps with very good spatiotemporal resolution. As the sensors used are not expensive, they could be deployed in areas that are not already covered by traditional rain measurement systems (rain gauges, radars), or in areas subject to strong rain impacts (for flash flood prevention, for instance).

Table 2. The statistical errors produced by the assimilation algorithm compared to the true initial rain map for the experiments shown in Figure 5.

	Entire Map		Rainy Areas		Dry Areas	
	RMSE (mm/h)	Bias (mm/h)	RMSE (mm/h)	Bias (mm/h)	RMSE (mm/h)	Bias (mm/h)
Sampling 10 s	0.84	+0.05	2.19	–0.04	0.24	–0.07
Sampling 1 min	1.03	+0.18	2.17	–0.18	0.39	+0.39
Sampling 5 min	1.52	+0.46	2.99	+0.07	0.69	+0.66

4. Conclusions

In this paper, we have introduced a new technique for retrieving rainfall maps at high spatiotemporal resolution. This method uses measurements of the attenuation affecting microwaves from TV satellites during their crossing of the atmosphere. These attenuation measurements – related by a power law to the mean rainfall rates over the Earth-satellite links and made by sensors located on the ground – are combined in a data-assimilation algorithm by a simple advection numerical model to propagate the rain fields through time. This technique allows retrieving the rainfall map at an initial time step that once propagated by the model is able to explain the observations recorded at different times.

This method was already successfully tested on real data sets recorded over a small area [11]. These encouraging results convinced us to go through larger areas, covered by many sensors.

In this paper, we showed results for simulated data on a realistic urban area. We proved the ability of our algorithm to deal with many sensors, and so to successfully retrieve rain maps over a quite larger area (30 km × 30 km). We have shown that this algorithm is able to deal with realistic instrumental noise, but that it needs observations with a very good time sampling (less than 1 min) to be run.

The next step in these developments consists in deploying a real system in an urban area, in order to validate the approach on real data over a city. The envisaged prototype would use 20 to 25 sensors and would be deployed over a medium-sized town, ideally subject to intense flash-flood events. This prototype experiment could be a first step before deploying this system in areas where no other classical and costly system is available.

5. References

1. A. Overeem, H. Leijnse and R. Uijlenhoet, "Country-Wide Rainfall Maps from Cellular Communication Networks," Proceedings of the National Academy of Sciences, **110**, 2013, pp. 2741-2745.

2. A. Berne and W. F. Krajewski, "Radar for Hydrology: Unfulfilled Promise or Unrecognized Potential?," *Advances in Water Resources*, **51**, 2013, pp. 357-366.

3. C. Chwala, A. Gmeiner, W. Qiu, S. Hipp, D. Nienaber, U. Siart, T. Eibert, M. Pohl, J. Seltmann, J. Fritz, and H. Kunstmann, "Precipitation Observation Using Microwave Backhaul Links in the Alpine and Pre-Alpine Region of Southern Germany," *Hydrology & Earth System Sciences*, **16**, 2012.

4. A. Doumounia, M. Gosset, F. Cazenave, M. Kacou, and F. Zougmore, "Rainfall Monitoring Based on Microwave Links from Cellular Telecommunication Networks: First Results from a West African Test Bed," *Geophysical Research Letters*, **41**, 2014, pp. 6016-6022.

5. A. Zinevich, H. Messer, and P. Alpert, "Frontal Rainfall Observation by a Commercial Microwave Communication Network," *Journal of Applied Meteorology and Climatology*, **48**, 2009, pp. 1317-1334.

6. M. Schleiss and A. Berne, "Identification of Dry and Rainy Periods Using Telecommunication Microwave Links," *IEEE Geoscience and Remote Sensing Letters*, **7**, 2010, pp. 611-615.

7. L. Barthès and C. Mallet, "Rainfall Measurement from the Opportunistic Use of an Earth-Space Link in the Ku Band," *Atmospheric Measurement Techniques*, **6**, 2013, pp. 2181-2193.

8. A. Maitra and K. Chakravarty, "Ku-Band Rain Attenuation Observations on an Earth-Space Path in the Indian Region," Proceedings of the URSI General Assembly, 2005.

9. D. Giuli, L. Facheris and S. Tanelli, "Microwave Tomographic Inversion Technique Based on Stochastic Approach for Rainfall Fields Monitoring," *IEEE Transactions on Geoscience and Remote Sensing*, **37**, 1999, pp. 2536-2555.

10. O. Bousquet, A. Berne, J. Delanoë, Y. Dufournet, J. Gourley, J. Van-Baelen, C. Augros, L. Besson, B. Boudevillain, O. Caumont et al., "Multifrequency Radar Observations Collected in Southern France During Hymex-sop1," *Bulletin of the American Meteorological Society*, **96**, 2015, pp. 267-282.

11. F. Mercier, L. Barthès and C. Mallet, "Estimation of Finescale Rainfall Fields Using Broadcast TV Satellite Links and a 4DVAR Assimilation Method," *Journal of Atmospheric and Oceanic Technology*, **32**, 2015, pp. 1709-1728.

12. E. Kalnay, *Atmospheric Modeling, Data Assimilation, and Predictability*, Cambridge, Cambridge University Press, 2003.

13. P. K. Smolarkiewicz, "A Simple Positive Definite Advection Scheme with Small Implicit Diffusion," *Monthly Weather Review*, **111**, 1983, pp. 479-486.

14. L. Nardi, C. Sorror, F. Badran and S. Thiria, "YAO: A Software for Variational Data Assimilation Using Numerical Models," Computational Science and Its Applications-ICCSA 2009, 2009, pp. 621-636.

15. J. C. Gilbert and C. Lemaréchal, "The Module m1qn3," INRIA Rocquencourt & Rhone-Alpes, 2006.

16. N. Akrour, A. Chazottes, S. Verrier, C. Mallet and L. Barthes, "Simulation of Yearly Rainfall Time Series at Microscale Resolution with Actual Properties: Intermittency, Scale Invariance, and Rainfall Distribution," *Water Resources Research*, **51**, 2015, pp. 7417-7435.